MLC quality assurance using EPID: A fitting technique with subpixel precision

Maria Mamalui-Hunter, Harold Li, and Daniel A. Low[a)]
Department of Radiation Oncology, Washington University School of Medicine, 4921 Parkview Place, St. Louis, Missouri 63110

(Received 1 August 2007; revised 11 March 2008; accepted for publication 9 April 2008; published 19 May 2008)

Amorphous silicon based electronic portal imaging devices (EPIDs) have been shown to be a good alternative to radiographic film for routine quality assurance (QA) of multileaf collimator (MLC) positioning accuracy. In this work, we present a method of acquiring an EPID image of a traditional strip-test image using analytical fits of the interleaf and leaf abutment image signatures. After exposure, the EPID image pixel values are divided by an open field image to remove EPID response and radiation field variations. Profiles acquired in the direction orthogonal to the leaf motion exhibit small peaks caused by interleaf leakage. Gaussian profiles are fitted to the interleaf leakage peaks, the results of which are, using multiobjective optimization, used to calculate the image rotational angle with respect to the collimator axis of rotation. The relative angle is used to rotate the image to align the MLC leaf travel to the image pixel axes. The leaf abutments also present peaks that are fitted by heuristic functions, in this case modified Lorentzian functions. The parameters of the Lorentzian functions are used to parameterize the leaf gap width and positions. By imaging a set of MLC fields with varying gaps forming symmetric and asymmetric abutments, calibration curves with regard to relative peak height (RPH) versus nominal gap width are obtained. Based on this calibration data, the individual leaf positions are calculated to compare with the nominal programmed positions. The results demonstrate that the collimator rotation angle can be determined as accurate as 0.01°. A change in MLC gap width of 0.2 mm leads to a change in RPH of about 10%. For asymmetrically produced gaps, a 0.2 mm MLC leaf gap width change causes 0.2 pixel peak position change. Subpixel resolution is obtained by using a parameterized fit of the relatively large abutment peaks. By contrast, for symmetrical gap changes, the peak position remains unchanged with a standard deviation of 0.05 pixels, or 0.026 mm. A trial run of 36 test images, each with gap widths varying from 0.4 to 1.4 mm, were used to analyze 8640 abutments. The leaf position variations were detected with a precision of 0.1 mm at a 95% confidence level, with a mean of 0.04 mm and a standard deviation of 0.03 mm. The proposed method is robust and minimizes the effect of image noise and pixel size and may help physicists to establish reliable and reasonable action levels in routine MLC QA. © *2008 American Association of Physicists in Medicine*. [DOI: 10.1118/1.2919560]

Key words: EPID, MLC QA, IMRT, Lorentzian fitting

I. INTRODUCTION

The rapidly growing number of intensity-modulated radiation therapy (IMRT) treatments calls for a quantitative, automated, and reliable multileaf collimator (MLC) quality assurance (QA) procedure that can be used routinely in the clinical setting. An important aspect of the MLC QA procedure is related to the positioning accuracy of the MLC leaves during the IMRT delivery.[1–3] The strip test devised by Chui *et al.*[3–7] has been widely used, and has proven to be a good approach to identify submillimeter leaf positioning errors. Briefly, this QA test consists of delivering multiple abutting radiation field segments. At each abutment, the right and left opposing leaf pairs are instructed to undertravel by 0.5 mm, producing a matrix of highly exposed regions on radiographic films. Because the dose delivered at the abutment region is sensitive to leaf positioning accuracy, small MLC leaf positioning errors can be evaluated even by visual inspections. Based on this strip test, Sastre-Padro *et al.*[7] developed a method that can be used for accurate MLC calibration. They were able to determine individual leaf offsets by quantifying the relative positioning error and absolute positioning error using radiographic film. The above-mentioned QA procedure is effective but can be labor intensive, time consuming, and limitations of the film size and MLC leaf travel require multiple measurements to validate that the leaf calibration is accurate for all MLC leaves and throughout their range of motion. Evaluating leaf motion accuracy as a function of gantry angle (to check the influence of gravity on MLC leaf calibration) requires repeated, time consuming measurements as well.

A recent study by Chang *et al.*[6] showed that an amorphous silicon based electronic portal imaging device (EPID) was a good alternative to radiographic film for this routine MLC QA procedure. An important advantage of using EPIDs over radiographic film is that the EPID images can be acquired, analyzed, and stored more rapidly and conveniently.

They also pointed out that the faulty pixels in EPID images could lead to erroneous determination of theses parameters if they were not properly handled.

Amorphous silicon based EPIDs have been investigated extensively for radiation therapy QA.[4,6,8–14] Excellent long-term consistency[11,15,16] and the availability on all new models of linear accelerators make them a promising tool for MLC QA. However, the differential energy response and the variation in sensitivity across the EPID[17,18] together with the pulsed feature of linear accelerator-based dose delivery[19] can superimpose significant artifacts on the EPID images, making dose evaluation less accurate, and consequently less useful. Although elegant denoising techniques can be applied,[4,10] useful information may be unintentionally removed. Furthermore, depending on the goals, the detection precision can also be compromised by the resolution of the digital data.

In this work we developed a method that allowed precise verification of individual MLC leaf positions using amorphous silicon EPIDs by extending the work of Chui *et al.*,[3] Chang *et al.*,[6] and Sastre-Padro *et al.*[7] The strip test image data was normalized by dividing by an open field image acquired at the same measurement session in order to remove potential variations in beam output and symmetry and minimize the effect of local EPID response variations. Features in the image that were associated with the MLC leaf orientation were used to correct for the relative orientation of the imager and MLC leaf carriages. The abutment peaks were automatically detected and fitted by parameterized functions that allowed a quantitative and automated determination of the MLC leaf positions. The use of functional fits reduced the sensitivity of this technique to image noise and pixel averaging and enabled subpixel leaf positioning detection.

II. MATERIALS AND METHODS

II.A. MLC and EPID

The measurements were performed on a multimodality linear accelerator (21EX, Varian Medical, Palo Alto, CA) with a 12 leaf MLC (Millennium, Varian Medical, Palo Alto, CA). The MLC consisted of two banks of 60 leaves: The central 40 leaves of each bank projected to 0.5 cm width, while the outer 20 leaves (ten on each side of the central segment) projected to 1.0 cm in the isocenter plane. The MLC had been calibrated according to the manufacturer specifications.

The portal imager (aS500, Varian Medical Systems, Palo Alto, CA) consisted of an array of 512×384 amorphous Si photodiodes, each connected to a thin film transistor for a separate readout of each diode's signal. A 0.3 mm gadolinium oxysulphide phosphor screen was placed over the photodiode plane to convert ionizing radiation to detectable light. A 1 mm thin copper plate upstream from the phosphor acted as an x-ray converter while preferentially attenuating low-energy photons. The physical pixel pitch of the imager was 0.78×0.78 mm^2. The EPID was mounted on a retractable arm that was calibrated to meet the manufacturer's alignment specifications. The imager was assumed not to cause any distortion.[9]

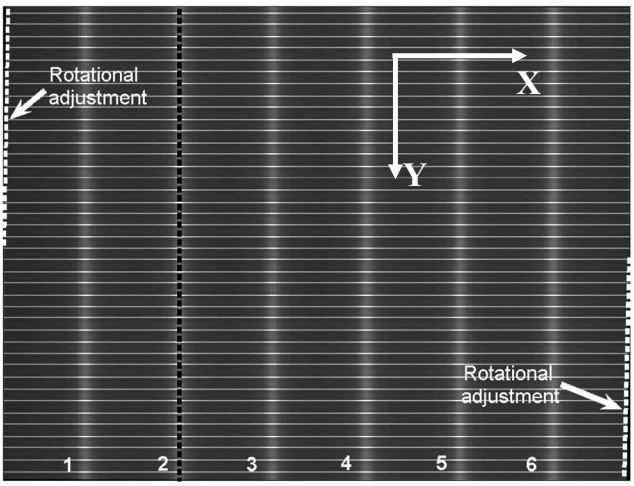

FIG. 1. (a) A strip test image acquired using an EPID. The dashed lines illustrate the effect of rotational correction (the rotational correction is exaggerated to highlight the influence of the rotational adjustment), black dashed vertical line indicates the position of the abutment; solid white horizontal lines indicate the position of interleaf leakage stripes.

II.B. Strip test

The collimator axis of rotation was used to define the coordinate system origin. It was determined by imaging a fixed, nominally 10×10 cm^2, field at three orthogonal collimator angles of 90°, 180°, and 270° (Varian convention) placing the EPID at a source-to-detector distance of 150 cm. The geometric center for each field was calculated based on locating the 50% isointensity level for the four field edges, and then averaging the field edge locations.

The strip test consisted of seven adjacent step-and-shoot segments of nominally 2 cm width (Fig. 1). The leaf gap was defined relative to successive segment irradiations. When the successive segment penumbrae are programmed to match exactly, the opposing leaf positions are set to the same location during the adjacent segments. The leaf gap then is described as being 0 mm. In this way, both positive and negative leaf abutments can be delivered, with the corresponding changes in shape and size of the overlapping penumbra peaks. Because not only the size of the abutment peaks changed as the leaf gap approached zero, but also the shape, it was decided, following the previous work,[3,6] to use a gap of 1 mm as the nominal standard gap and determine the peak shape and size variation with respect to the nominal 1 mm gap settings.

An IMRT portal imaging acquisition mode was employed to collect the imaging data. During radiation delivery, a continuous acquisition of image frames was obtained. At the end of acquisition, a 14 bit image was automatically created by averaging all the frames.[9] All the images were taken using 100 monitor units. The number of integrated EPID frames, ranging from 212 to 216, was recorded by the system and written to the image header.

For our experiments, the image data were acquired at a source-to-detector distance of 150 cm and the pixel size was scaled by 1.5^{-1} to correspond to the radiation field size at 100 cm from the source. A nominal dose rate of 300 MU min^{-1} was used. The subsequent images contained 240 individual leaf pair abutments (40 leaf pairs $\times 6$ abutments) that were analyzed to determine the MLC position characteristics. A dark-field image was acquired and an open-field image was taken by opening the MLC to 14×20 cm^2. These were used to account for changes in beam radiation distribution characteristics and variations of the EPID response.

Using a method similar to that of Sastre-Padro *et al.*,[7] the following formulas were used to calculate the leaf positions from the strip-test abutment peaks:

$$x_{B\_ij} = \frac{g_{ij}}{2} - (x_{ij}^{0} - x_{i}^{\text{abut}}) \tag{1}$$

$$x_{A\_ij} = g_{ij} - x_{B\_ij}, \tag{2}$$

where x_{B_ij} and x_{A_ij} were the leaf positions of the jth ($j = 1, 2, \ldots, 40$) leaf pair relative to the average ith ($i = 1, 2, \ldots, 6$) abutment position for B bank and A bank, respectively, x_{ij}^{0} was the peak position of the jth leaf pair at the ith abutment, x_{i}^{abut} was the average position of abutment i, and g_{ij} was the gap width on the abutment i for the leaf-pair j.

For clarity, the leaf positions were labeled using the notation of Chui *et al.*[3] In that notation, the leaf positions relative to the intended gap center were identified separately for each leaf bank. For example, the nominal gap of 1 mm is labeled as (0.5, 0.5), which indicates that each leaf bank is programmed to undertravel to a position 0.5 mm away from the gap centerline, leading to the 1.0 mm gap.

II.C. Image analysis

The strip-test images were analyzed in the following steps. In this work the x and y position coordinates are defined in the direction of and perpendicular to the leaf motion, respectively (Fig. 1).

II.C.1. Image preprocessing

The images were processed to correct for individual pixel sensitivity offsets and gains. The processed image I_{proc} was determined using

$$I_{\text{proc}} = \frac{I_{\text{raw}} - I_{\text{dark}}}{I_{\text{open}} - I_{\text{dark}}}, \tag{3}$$

where I_{raw} was the raw strip-test image, I_{dark} was a dark field image that was acquired without irradiation and served as an offset correction, and I_{open} was the open-field image.

II.C.2. Image alignment

The acquired EPID images were rotated to align to the collimator assembly. Using a process similar to that of Budgell *et al.*[4] and Bayouth *et al.*,[5] the rotation angle was computed by examining the MLC interleaf leakage dose signature. We selected an arbitrary number of equally spaced pixel columns (100 were used in this work) that were nominally perpendicular to the leaf travel direction (i.e., y direction as shown in Fig. 1). The locations of all MLC leaf pairs (their y coordinates) were automatically identified. The image profile along each column contained image peaks due to the interleaf leakage. The shape of the peaks was well described by a Gaussian function, which was used to identify the centroid of each of the 39 interleaf junctions along each pixel column. The relative rotation angle between the EPID image and the MLC was determined iteratively using a multiobjective minimization function based on the assumption that for an aligned collimator, the leakage peaks between adjacent pairs of leaves would lie parallel to the pixel rows. We utilize the *fgoalattain* function from MATLAB™ (MathWorks, Inc.) to optimize the fitting parameters. This function is based on a sequential quadratic programming method and solves the goal attainment problem.[20]

II.C.3. Leaf abutment quantitation

Using the aligned image and the positions of the MLC pairs, profiles along the x direction were extracted along the central portion of each leaf pair. To improve the noise characteristics of the profiles, the central and two neighboring pixel rows (± 0.78 mm) were averaged. Within the 40 profiles lay the 240 abutment peaks.

The locations of the 240 abutment peaks were identified using an automated search routine. It was determined heuristically that the shape of the peaks was well described using a modified Lorentzian function

$$L(x) = (a \cdot x + b) + \frac{s}{\pi} \cdot \frac{\Gamma/2}{(x - x_0)^2 + (\Gamma/2)^2}, \tag{4}$$

where s, x, x_0, and Γ had units of length, a had units of $(\text{length})^{-1}$, and b was dimensionless. The parameter x_0 represented the position of the dose peak, s was the scaling factor, and Γ was analogous to FWHM of a classic Lorentzian function. Note that a linear term was added to the Lorentzian function to allow the function to more accurately describe the base line dose near the abutment region. The dose peaks were typically asymmetric, especially near the field edges, and were due, in part, to the variations in delivered MUs and to programmed abutment position variations. The asymmetry of the dose peak tails is demonstrated on the typical strip test intensity profile taken in the direction parallel to the leaf motion (Fig. 2). We defined relative peak height (RPH) as

$$RPH = L(x_0) - (a \cdot x_0 + b). \tag{5}$$

In order to determine the gap width g_{ij} in the Eqs. (1) and (2), a calibration curve that characterized the relationship between RPH and nominal gap width was required. The RPH calibration should be conducted immediately after the MLC leaves have been calibrated (with an accuracy of 0.05 mm). First, 11 strip test images with nominal gap width ranging from 0.0 to 2.0 mm were acquired. Each image contained

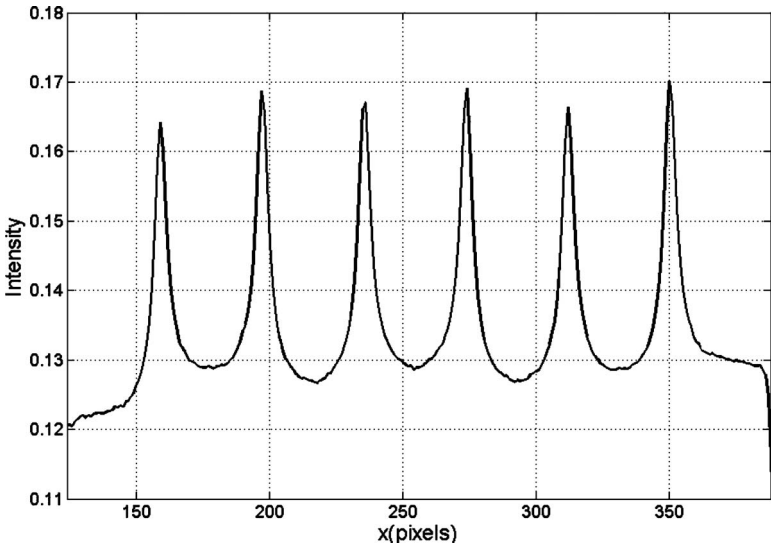

FIG. 2. Typical intensity profile of a strip test image in the direction parallel to the leaf motion.

only one nominal gap width. The gaps were formed symmetrically by equally under-traveling leaf banks in opposite directions. Each image contained 40 peaks times six abutments totaling 240 abutments. Second, each abutment peak for each leaf pair was fitted with Eq. (4), and the corresponding RPH values were extracted. Third, the average RPH over 40 leaf pairs was calculated for each abutment, and became the "golden standard" RPH for the nominal gap width at the particular abutment. Finally, six calibration curves were obtained as there were six abutments. For each of the six abutments, the 11 RPH data points were fitted with a fourth order polynomial: $\mathrm{RPH}(g)=c_0+c_1g+c_2g^2+c_3g^3+c_4g^4$, where g and $\{c_i\}_{i=1,\ldots,4}$ were nominal gap width and polynomial coefficients, respectively.

The second set of 11 EPID images for asymmetrically formed gaps was also acquired with the same gap widths. Asymmetric gaps were formed by under traveling of a single leaf bank relative to the nominal abutment position. The purpose was to test whether RPH versus gap width behavior was dependent of how the gap is formed.

II.C.4. Assessment of the technique

In order to test the upper level of precision of this technique, nominal abutment gaps, ranging from 0.4 to 1.4 mm wide with a range of combinations of A and B bank leaf settings, were created. For example, the 0.8 mm gap was formed using five combinations of MLC settings: (0, 0.8), (0.2, 0.6), (0.4, 0.4), (0.6, 0.2), (0.8, 0.0). Altogether 36 test images were acquired to make up the test image suite, each using a unique MLC setting. The measured leaf positions were compared against the nominal ones.

III. RESULTS

III.A. Image alignment

The alignment process used 100 pixel columns to determine the relative collimator orientation, but it was discovered that the interleaf leakage analysis was not robust near the leaf abutments. Therefore, these pixel columns were ignored in the alignment process.

Figure 3 shows the measured relative angle between the MLC leaves and the EPID pixel rows for the 36 images from the test series. The images required about 20 min to acquire and the average rotation angle was approximately 0.2°. Images 1 through 6 have an average angle of −0.24° and images 7 through 36 have an average angle of −0.19°. Individually both sets of images exhibit a standard deviation of 0.01°. Based on the relatively small standard deviation for each subset of images, we believe this 0.05° difference between the mean angles of the two subsets was caused by a mechanical process (e.g., angular drift of either the linear accelerator head or the EPID itself, although no personnel entered the room during the image acquisition sequence).

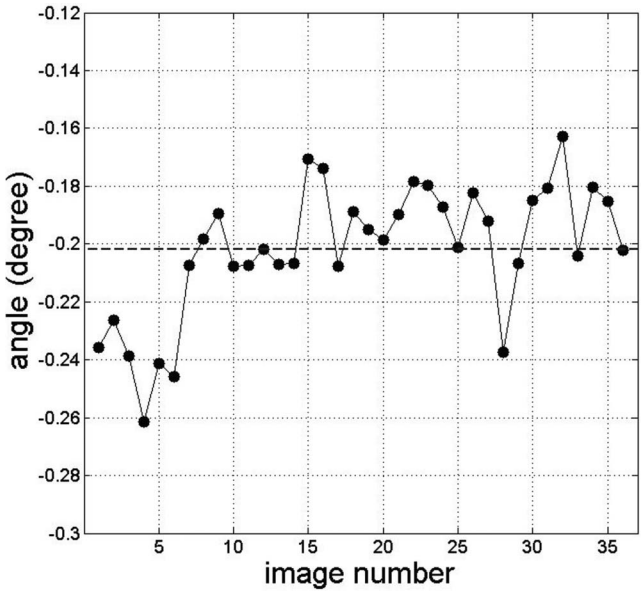

FIG. 3. Image rotation angle for 36 EPID images from the test series.

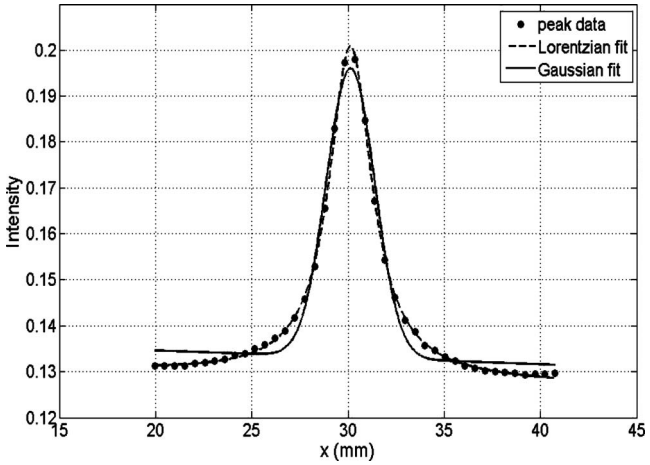

FIG. 4. Measured abutment peak and corresponding Lorentzian and Gaussian function fits.

III.B. Leaf abutment quantitation

Figure 4 compares a Lorentzian fit to a Gaussian fit for a measured dose profile on one of the abutments. The dose profile falls off more slowly in the penumbra region and the peak height is lower than a Gaussian model can describe. By contrast, the modified Lorentzian function fits the data quite well. To quantify the fit quality, we calculated the root-mean-square percentage errors (RMSPEs) about the fitted peak value for the two functions. RMSPE is defined as: $\mathrm{RMSPE} = \mathrm{RPH}^{-1}(N^{-1}\Sigma_N(Fit-Data)^2)^{1/2}$. Our results show that Lorentzian fitting consistently yielded smaller RMSPE values. As an example, for a nominal gap of 1 mm and five MLC settings [(0.0, 1.0), (0.2, 0.8), (0.4, 0.6), (0.6, 0.4), (0.8, 0.2), and (1.0, 0,0)], the RMSPE was 0.0036 ± 0.0004 (1σ) for the Lorentzian, while for the Gaussian the RMSPE was about five times greater: 0.016 ± 0.0005 (1σ).

III.C. RPH calibration

Figures 5(a) and 5(b) show the impact of varying the gap width and the gap position on the dose profile, respectively. Because of the analytic fitting process, influence on the RPH determination from image noise and the finite pixel resolution are reduced. The calibration curves that relate the nominal gap width to the RPH are shown in Fig. 6(a) for each of the six abutments (shown in Fig. 1). Solid lines represent the fourth-order polynomial fit for the symmetric case, and dashed lines represent the asymmetric case. In each case, the preset nominal gaps vary from 0.0 to 2.0 mm, and the error bars show the single standard deviation of the RPH values for the specific nominal gap. Figure 6(b) shows the same data overlaid to show the variation from abutment to abutment. As seen in Fig. 6, a change in gap width of 0.2 mm leads to a change in RPH of about 10%. At each of six abutments, the two calibration curves overlie each other closely, indicating that the RPH value is a function of gap width only, and is independent of how the gap is created. For each calibration curve the standard deviation is approximately 3% of the mean RPH as derived using the 40 MLC leaf pairs.

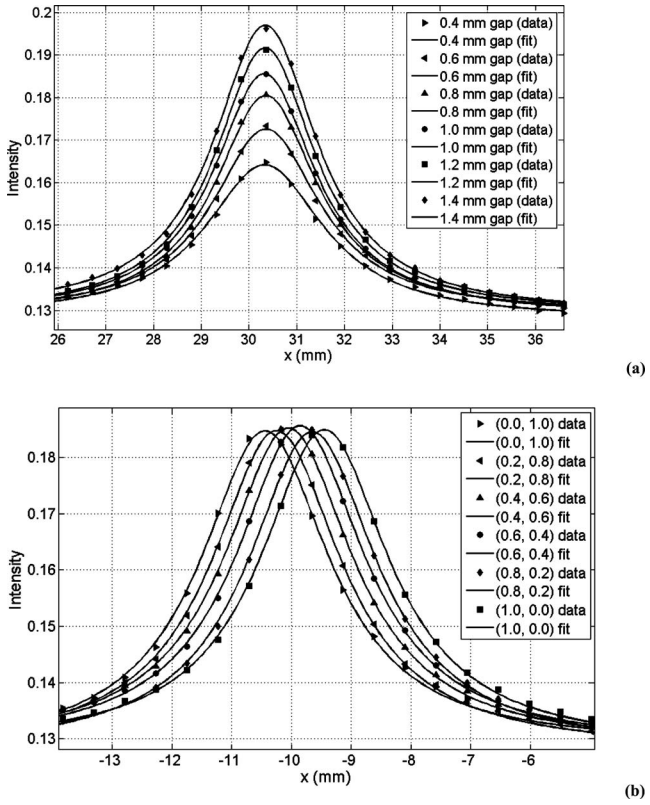

FIG. 5. Measured abutment peak: (a) Peak height dependence on the nominal gap width. The labeled data points and corresponding solid lines represent the image pixel data and fits, respectively, for 0.4 mm, 0.6 mm, 0.8 mm, 1.0 mm, 1.2 mm, and 1.4 mm nominal gap widths, (b) Variation of peak position for a set of asymmetrically varying leaf positions.

Based on the RPH calibration datasets, the differences between the nominal gap width and measured gap width were calculated for the 8640 dose peaks (240 peaks per image $\times 36$ images) from the test series. The mean gap difference was $0.06\ \mathrm{mm} \pm 0.02\ \mathrm{mm}$. The measured versus nominal gap width is plotted in Fig. 7.

III.D. Peak position

For the asymmetrically produced gaps, the peak position shifted proportionally with the increase of gap width (Fig. 8). On average, a 0.2 mm gap width change causes a 0.2 pixel peak position change (EPID positioned at 150 cm SSD results in pixel size of 0.52 mm). As expected, the symmetrical gaps' peak position remained unchanged with a standard deviation of 0.05 pixels, or 0.026 mm.

III.E. Measured versus preset leaf positions

The measurement of the leaf peak position and the gap width allows each leaf bank position to be determined separately. This is shown in Fig. 9, where the results of each of the 36 images in the image test suite are plotted with unique symbols. Each of the 240 abutment points in each image

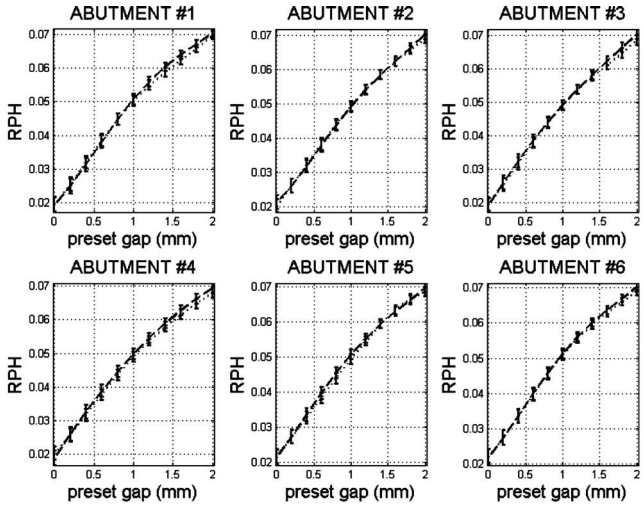

(a)

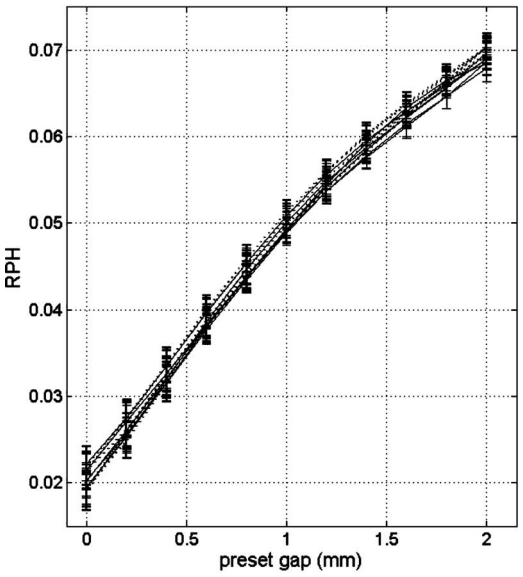

(b)

FIG. 6. (a). RPH vs nominal gap width for the six abutment regions in the seven-field strip test. Both symmetric and asymmetric gaps are displayed as solid and dashed lines, respectively, for a series of measurements with varying gap widths. The standard deviations correspond to the variation in the RPH measurements for the 40 MLC leaf pairs, (b) Superimposed curves from Fig. 6(a), showing the spread of the NPH curves for the six abutment regions. Solid lines: Symmetric gap. Dashed lines: Asymmetric gap.

determined an A and B leaf position and is marked by a point. The data are clustered near the nominal leaf position values. Overall, the mean and standard deviation of absolute value of difference between the measured and nominal leaf positions was 0.04 mm $\pm$ 0.03 mm(1σ). Figure 10 shows the differential histograms of the difference between the nominal and measured leaf positions for the two leaf banks. For A and B bank leaves, 95% of calculated positions are within 0.11 and 0.13 mm of nominal ones, respectively.

IV. DISCUSSION

In this work we have presented a process of using an amorphous-silicon EPID imager and a commonly used MLC irradiation sequence, the conventional strip test, to quantitate the MLC leaf position during step-and-shoot IMRT delivery. The method uses empirical functional fits to the MLC interleaf leakage and abutment dose distributions. The use of ana-

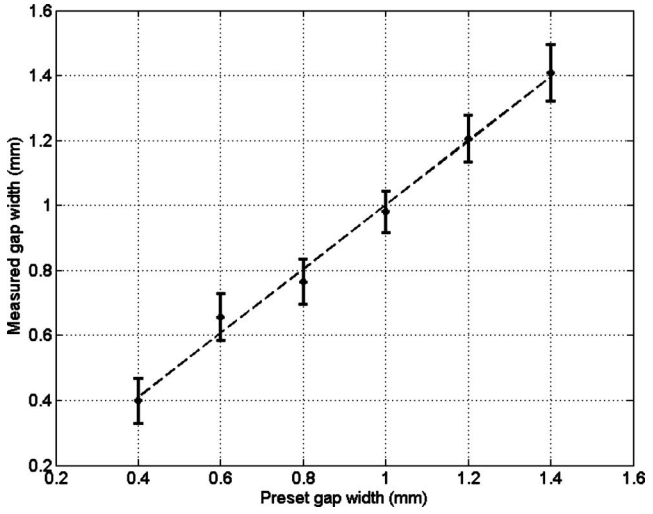

FIG. 7. Measured vs preset gap width for gap widths ranging from 0.4 to 1.4 mm.

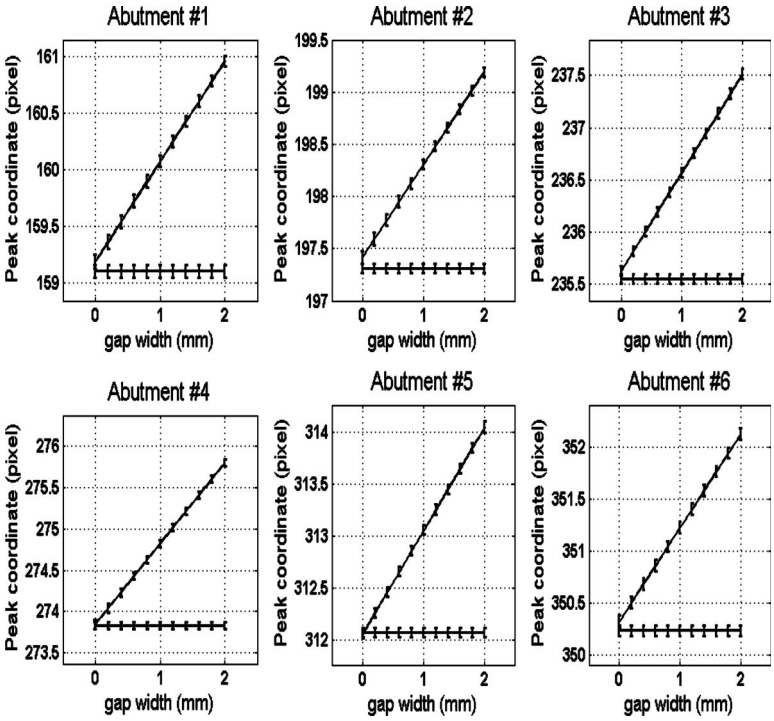

FIG. 8. X_0 vs asymmetric gap (upper) and symmetric gap for six abutments.

lytic fitting rather than direct pixel-by-pixel analysis reduces the impact of image noise and allows quantitative results with subpixel resolution.

This technique uses the strip test[3] consisting of six abutments (seven fields) with a nominal 2 cm separation. A relative MLC and imager rotation correction was necessary to accurately identify the source of subsequent abutment offsets as MLC calibration errors. This was accomplished by detecting and quantifying the positions of the MLC interleaf leakage dose peaks. As mentioned in Sec. II B, the algorithm began by identifying 100 equally spaced profiles aligned along the imager's y axis, detecting the peak positions and fitting the detected leakage peaks using Gaussian functions. The peaks that overlay the abutment gaps had significantly different shapes, and the fitting results for those regions were unreliable. Therefore, the near-abutment peaks were removed from the set of the peak coordinates used for calculating the collimator rotation angle for each image.

We used 1 mm nominal gap width for the routine MLC QA procedure as suggested by other authors.[3,6] To design an

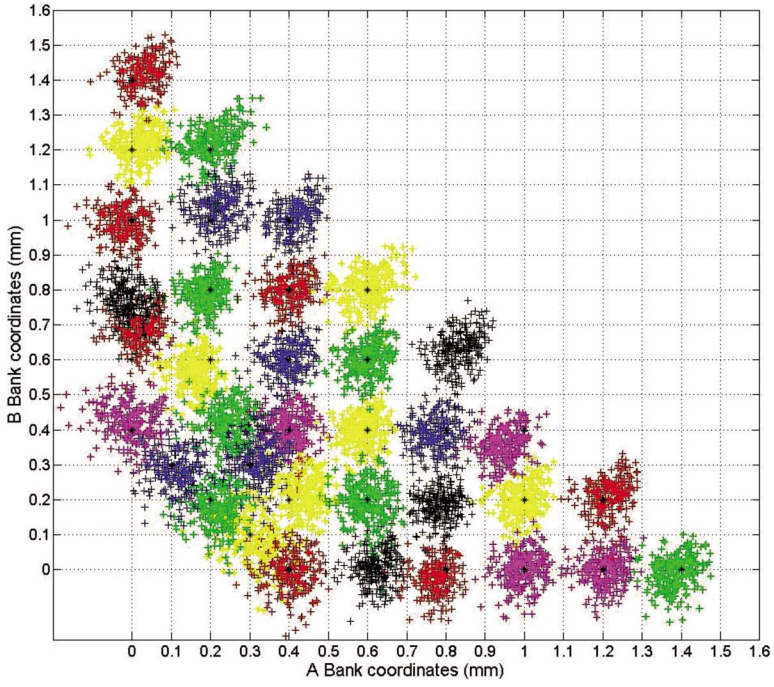

FIG. 9. Scatter plot of measured vs preset leaf position. Each cloud consists of 240 data points (40 leaf pairs × six abutments).

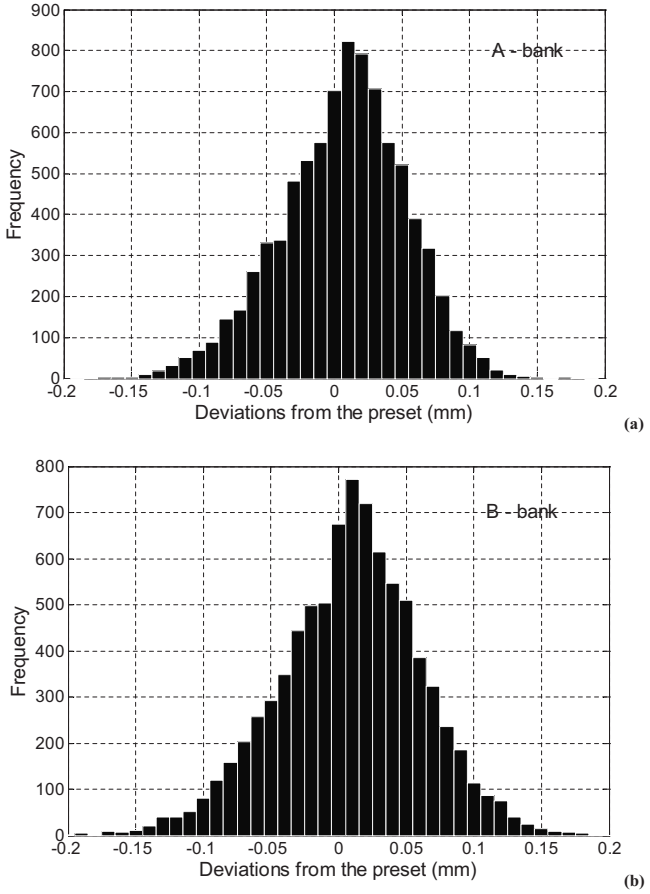

FIG. 10. Frequency histogram of data presented in Fig. 9.

automated procedure, finding the correct analytical form for the dose peaks is essential. We found that setting the nominal gap to 1.0 mm ensured that the overall shape of the abutment dose peak was consistent for gaps ranging from 0.0 to 2.0 mm and, therefore, allowed this technique a relatively wide latitude for automatically and quantitatively determining the gap width.

While the validated gap width variation was ± 1 mm, a greater gap width variation might be encountered in clinical practice. The automated routine would not quantitatively determine a gap larger than the gaps tested here, but could be made to detect such a relatively large leaf positioning error and identify it to the medical physicist.

These results show that, when a suitable analytical function was fitted to the detected dose peak, the formulas of Sastre-Padro *et al.*[7] provided an accurate estimation of the individual leaf position. The automated method provided a leaf calibration error to a precision better than 0.2 mm. This met the tolerance limit of 0.2 mm for leaf positioning accuracy suggested by other authors.[1,21]

The use of an open-field image to normalize the strip-test image reduced the influence of radiation field variation on the subsequent analysis. Budgell *et al.*[4] implied that dividing the strip test image by a daily open-field image could introduce more noise into the analysis. Therefore, they did not include this step in their approach. Since our method is based on analytic fitting, the analysis is much less affected by the noise; thus, the process capitalizes the potential advantages of this procedure, which makes automated and robust routine MLC QA possible.

In a recent study, Yang and Xing[14] showed that for some leaf position measurement analysis techniques the position of neighboring leaf pairs affects the measurement of leaf positions. We investigated the magnitude of influence on our technique by varying the gap widths for neighboring leaf pairs (two on each side) from 0.0 to 3.6 mm with central leaf pair staying at a constant gap of 0.6 mm. We found that the change of RPH was less than 1%, which translated to about a 0.02 mm uncertainty in gap width determination. Thus, the cross-talk effect was considered negligible for our procedure.

It is noted that the accuracy of any strip test based MLC QA procedure relies on the segment to segment MU reproducibility. Even with the linear term in the modified Lorentzian functional fit, a 2% segment-to-segment MU delivery inconsistency would cause a leaf abutment position measurement error of 0.1 mm. Therefore, full automation of this technique will require an analysis of the intensity of each segment to determine if the MUs are delivered within 2% of the neighboring segments. Alternatively, an analysis of the influence of delivery error on the abutment determination could be conducted to correct the measurement error. Finally, dose delivery errors for segmental IMRT delivery have typically been small when the number of MUs exceeds 20 MU, so specifying a minimum number of MUs per segment would typically limit the delivery error. In this case, the relative intensity of each segment could be monitored to assure that the delivery intensity was within tolerance (e.g., 2%).

The method presented here requires measuring RPH versus nominal gap width calibration curves (shown in Fig. 6). This may be conducted immediately after the MLC leaves have been accurately calibrated or after servicing procedures. For routine MLC QA, for example, a weekly MLC test, four images are required to be taken by the QA staff: one strip test image with 1 mm gap width, one MLC-shaped open-field image for the normalization according the Eq. (3) and two images of the open fields formed by symmetric jaws at 90° and 270° collimator angles for determining the collimator axis of rotation. In order to cover the entire 120 leaves of a Varian Millennium™ MLC the strip-test image can be acquired with collimator at 90° and a 100 cm source-to-detector distance to take advantage of the 40 cm physical width of an on-board Varian EPID. The method has been implemented using MATLAB™ code. It takes about 30 min to analyze one strip-test image. The computing time can be reduced considerably by employing a lower-level computer language and more efficient programming routines.

V. CONCLUSIONS

In this work we report a technique that is an important step towards quantitative and automated MLC positioning QA. Subpixel precision was achieved by fitting interleaf and abutment peaks of the common picket-fence test to Gaussian and Lorentzian functions, respectively. The image relative

rotation angle was determined with a precision of 0.01° by using the interleaf leakage peaks and an optimization technique. The MLC leaf positions can be determined with a precision of 0.1 mm at the 95% confidence level, 0.04 mm on average with a standard deviation of 0.03 mm. Clinical implementation would require an initial independent leaf calibration verification method (such as direct caliper measurements) to calibrate the peak height-to-leaf gap curve. Otherwise, the test is useful as a detector of MLC calibration variation relative to the initial measurement set.

ACKNOWLEDGMENT

This work is supported in part by a grant from Varian Medical Systems.

[a]Author to whom correspondence should be addressed. Electronic mail: dlow@radonc.wustl.edu

[1]T. LoSasso, C. S. Chui, and C. C. Ling, "Physical and dosimetric aspects of a multileaf collimation system used in the dynamic mode for implementing intensity modulated radiotherapy," Med. Phys. **25**, 1919–1927 (1998).

[2]D. A. Low, J. W. Sohn, E. E. Klein, J. Markman, S. Mutic, and J. F. Dempsey, "Toward automated quality assurance for intensity- modulated radiation therapy," Int. J. Radiat. Oncol., Biol., Phys. **53**(2), 443–452 (2002).

[3]C. S. Chui, S. Spirou, and T. LoSasso, "Testing of dynamic multileaf collimation," Med. Phys. **23**, 635–641 (1996).

[4]G. J. Budgell, Q. Zhang, R. J. Trouncer, and R. I. Mackay, "Improving IMRT quality control efficiency using an amorphous silicon electronic portal imager.," Med. Phys. **32**(11), 3267–3278 (2005).

[5]J. E. Bayouth, D. Wendt, and S. M. Morrill, "MLC quality assurance techniques for IMRT applications," Med. Phys. **30**, 743–750 (2003).

[6]J. Chang, C. Obcemea, J. Sillanpaa, J. Mechalakos, and C. Burman, "Use of EPID for leaf position accuracy QA of dynamic multileaf collimator DMLC treatment," Med. Phys. **31**, 2091–2096 (2004).

[7]M. Sastre-Padro, U. A. van der Heide, and H. Welleweerd, "An accurate calibration method of the multileaf collimator valid for conformal and intensity modulated radiation treatments," Phys. Med. Biol. **49**(12), 2631–2643 (2004).

[8]S. J. Baker, G. J. Budgell, and R. I. MacKay, "Use of an amorphous silicon electronic portal imaging device for multileaf collimator quality control and calibration," Phys. Med. Biol. **50**, 1377–1392 (2005).

[9]A. Van Esch, T. Depuydt, and D. P. Huyskens, "The use of an aSi-based EPID for routine absolute dosimetric pre-treatment verification of dynamic IMRT fields," Radiother. Oncol. **71**, 223–234 (2004).

[10]S. C. Vieira, M. L. Dirkx, K. L. Pasma, and B. J. Heijmen, "Fast and accurate leaf verification for dynamic multileaf collimation using an electronic portal imaging device," Med. Phys. **29**, 2034–2040 (2002).

[11]P. B. Greer and C. C. Popescu, "Dosimetric properties of an amorphous silicon electronic portal imaging device for verification of dynamic intensity modulated radiation therapy," Med. Phys. **30**, 1618–1627 (2003).

[12]J. Chang and C. C. Ling, "Using the frame averaging of aS500 EPID for IMRT verification," J. Appl. Clin. Med. Phys. **4**, 287–299 (2003).

[13]B. M. C. McCurdy, K. Luchka, and S. Pistorius, "Dosimetric investigation and portal dose image prediction using an amorphous silicon electronic portal imaging device," Med. Phys. **28**(6), 911–924 (2001).

[14]Y. Yang and L. Xing, "Quantitative measurement of MLC leaf displacements using an electronic portal image device," Phys. Med. Biol. **49**, 1521–1533 (2004).

[15]L. N. McDermott, R., J. W. Louwe, J.-J. Sonke, M. B. van Herk, and B. J. Mijnheer, "Dose–response and ghosting effects of an amorphous silicon electronic portal imaging device," Med. Phys. **31**, 285–295 (2004).

[16]Y. El-Mohri, L. E. Antonuk, J. Yorkston, K.-W. Jee, M. Maolinbay, and K. L. Lam, "Relative dosimetry using active matrix flat-panel imager (AMFPI) technology," Med. Phys. **26**(8), 1530–1541 (1999).

[17]P. B. Greer, "Correction of pixel sensitivity variation and off-axis response for amorphous silicon EPID dosimetry," Med. Phys. **32**(12), 3558–3568 (2005).

[18]C. Kirkby and R. Sloboda, "Consequences of the spectral response of an a-Si EPID and implications for dosimetric calibration," Med. Phys. **32**(8), 2649–2658 (2005).

[19]O. A. Zeidan, J. G. Li, M. Ranade, A. M. Stell, and J. F. Dempsey, "Verification of step-and-shoot IMRT delivery using a fast video-based electronic portal imaging device," Med. Phys. **31**, 463–476 (2004).

[20]F. W. Gembicki, "Vector optimization for control with performance and parameter sensitivity indices," Ph.D. Dissertation, Case Western Reserve University, Cleveland, OH, 1974.

[21]J. R. Palta, S. Kim, J. G. Li, and C. Liu, "Tolerance limits and action levels for planning and delivery of IMRT," in *Intensity-Modulated Radiation Therapy: The State of the Art*, edited by J. R. Palta and T. Rockwell Mackie (Medical Physics, Madison, 2003), pp. 592–610.